LAWRENCE
LIVERMORE
NATIONAL
LABORATORY

LLNL-TR-713678

Radiation-induced aging of PDMS Elastomer TR-55: a summary of constitutive, mesoscale, and population-based models

A, Maiti, T. H. Weisgraber, L. N. Dinh

December 8, 2016

Disclaimer

This work performed under the auspices of the U.S. Department of Energy by Lawrence Livermore National Laboratory under Contract DE-AC52-07NA27344.

Radiation-induced aging of PDMS Elastomer TR-55: a summary of constitutive, mesoscale, and population-based models

A. Maiti, T. H. Weisgraber, L. N. Dinh

Abstract:

Filled and cross-linked elastomeric rubbers are versatile network materials with a multitude of applications ranging from artificial organs and biomedical devices to cushions, coatings, adhesives, interconnects, and seismic-isolation-, thermal-, and electrical barriers External factors like mechanical stress, temperature fluctuations, or radiation are known to create chemical changes in such materials that can directly affect the molecular weight distribution (MWD) of the polymer between cross-links and alter the structural and mechanical properties. From a Materials Science point of view it is highly desirable to understand, effect, and manipulate such property changes in a controlled manner. In this report we summarize our modeling efforts on a polysiloxane elastomer TR-55, which is an important component in several of our systems, and representative of a wide class of filled rubber materials. The primary aging driver in this work has been γ-radiation, and a variety of modeling approaches have been employed, including constitutive, mesoscale, and population-based models. The work utilizes diverse experimental data, including mechanical stress-strain and compression set measurements, as well as MWD measurements using multi-quantum NMR.

Notation:

λ = stretch ratio = $1 + \varepsilon$, where ε = engineering strain
$\lambda > 1$ → Tensile strain, $\lambda < 1$ → Compressive strain
$\lambda_1 =$ constant strain at which the material is exposed to radiation

Experimental stress-strain data under radiation at zero strain ($\lambda_1 = 1$)

Thin samples (0.1 mm x 10 mm x 40 mm) were exposed to γ-radiation from a Co-60 source (1.4MeV, 0.5Mrad/hour dose rate) as a convenient, controllable degradation pathway. The samples were irradiated in a nitrogen atmosphere until the desired dosage was reached, and then subjected to mechanical analysis (Fig. 1) using a TA Instruments ARES LS-2 rheometer in torsion rectangle geometry. Measurements were made in the dynamic oscillatory shear mode at room temperature using a frequency of 1 Hz (6.28 Rad/s). Strain was systematically incremented from the starting value (0.1%) to the end value (10%) using logarithmic spacing.

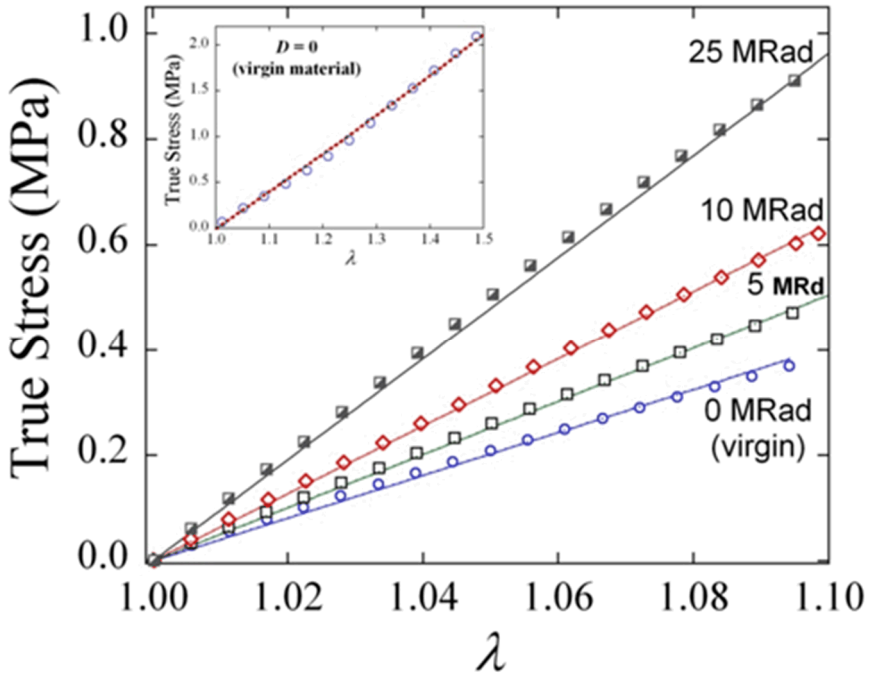

Figure 1. Stress-strain response of TR-55 subjected to different radiation dosages. Data is limited to stretch ratio (λ) of 1.1 or less. Experimental data (symbols) are displayed along with fits (lines) using the Neo-Hookean model, eq. (1) in text. Inset: Stress-strain response of the virgin material ($D = 0$) up to larger stretches ($\lambda \leq 1.5$) along with the Neo-Hookean fit (dashed line) with $G = 1.35$ MPa.

The above stress-strain data (up to moderate strains) can be accurately fit by the Neohookean model:

$$\sigma(\lambda) = G(\lambda^2 - 1/\lambda) \qquad (1)$$

as shown in Fig. 1. In eq. (1) G is the shear modulus that is proportional to ν_0, the volume density of chain segments between cross-links (and other physical restraints) with the proportionality constant depending on the details of the

network (i.e., bond-coordination of the junctions, the fraction and nature of fillers, etc.). The best fits of the experimental data (symbols) in Fig. 1 by eq. (1) yields the experimental shear modulus (G), plotted in Fig. 2 (symbols) as a function of radiation dosage D, along with errors due to sample-to-sample variation. The fit to the stress-strain response of the virgin material (Fig. 1 inset) yields a shear modulus of G_0 = 1.35 MPa. Fig. 2 shows that the shear modulus G increases, almost linearly, as a function of radiation (within our maximum dosage of 25 Mrad), implying a net increase in chain-segment density proportional to D.

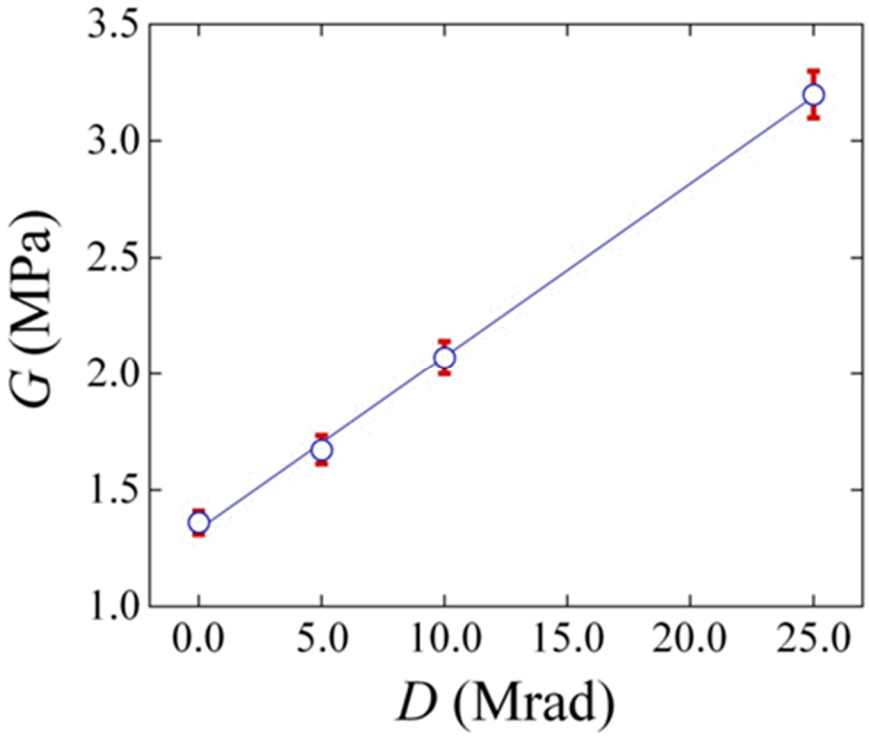

Figure 2. A plot of the shear modulus (G) from Neo-Hookean fits to the data in Fig. 1 as a function of radiation dosage (D). Errors bars in G are due to sample-to-sample variation. The solid line is a linear fit to the data.

Permanent Set measurements:

Experimental stress-strain data under radiation at non-zero tensile strains ($\lambda_1 > 1$):

To gain possible insight into the relative importance of bond-scission versus cross-linking events a second set of experiments were performed in which several samples were irradiated *while* being under pre-defined constant tensile strain (λ_1 = 1.20, 1.47, 1.67, 1.84). Upon reaching the desired dosage, the samples were removed from the irradiation chamber, released from tensile strain, and allowed to relax at ambient conditions for a week. The relaxed samples were then measured for the new equilibrium length, called the recovered length λ_s (symbols in figure 3), which is expressed as a ratio of the original (i.e. pre-exposure) equilibrium length [Note: Permanent set (P_s), a commonly used term in this context, is related to λ_s through the equation $P_s = (\lambda_s - 1)/(\lambda_1 - 1)$]. As shown in Fig. 3, λ_s increases as a function of both λ_1 and the radiation dosage D.

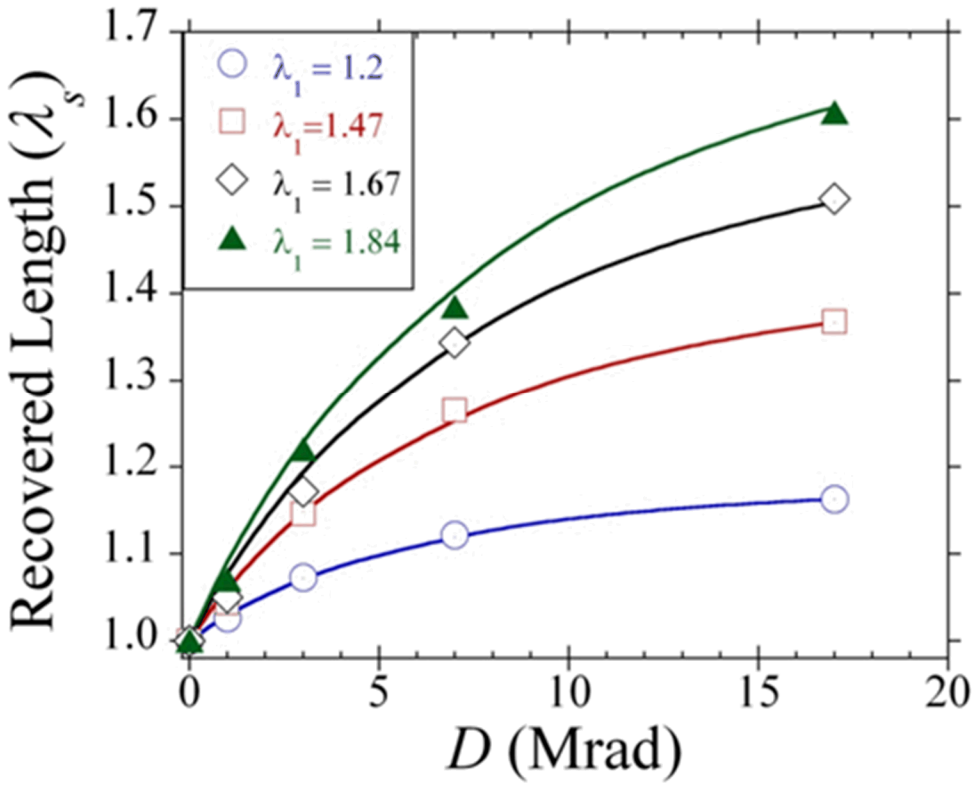

Figure 3. Permanent set data for TR-55 (expressed as recovered length (λ_s)) as a function of radiation dosage for different values of tensile stretch ratios (λ_1) at which the material is subjected to radiation. Solid lines are theoretical results using λ_1-independent f_{eff} (solid curve in figure 4(top) below) in eq. (5).

For a quantitative interpretation of Fig. 3, we adopt a two-stage independent network model originally proposed by Tobolsky [1], in which the rubber consists of: (1) the original network at an equilibrium length of 1 (i.e. zero strain), a fraction of which gets *modified* by radiation (either through cross-linking or through bond-scission), and (2) a new network created by radiation-induced cross-linking at an equilibrium length of λ_1. For concreteness of analysis let us assume an initial chain-segment-density of ν_0, a fraction f_{mod} of which gets modified by radiation. Let us also assume that the new network has a chain-segment-density ν_1, which as a fraction of the original chain density can be expressed as $\nu_1 = f_{xl}\nu_0$. In the presence of bond-scission (and λ_1 different from 1) there is an additional feedback effect (due to physical network relaxation) in which a part Φ of the new network (called the transfer function) relaxes back into the original network. In this case, the *effective* number of chain-segment-density in the two networks become [2] $\nu_0(1-f'_{mod})$ and $\nu_0 f'_{xl}$ respectively, where $f'_{mod} = f_{mod} - \Phi f_{xl}$ and $f'_{xl} = (1-\Phi)f_{xl}$. For a phantom network the transfer function can be approximated by the expression [3] $\Phi = \xi_{sci} f_{mod}/(1+f_{xl})$, where ξ_{sci} is the fraction of the original chain segments that are modified by scissioning. In the presence of the two networks eq. (1) gets modified to:

$$\sigma(\lambda) = G_0\left\{(1-f'_{mod})\left(\lambda^2 - \frac{1}{\lambda}\right) + f'_{xl}\left(\frac{\lambda^2}{\lambda_1^2} - \frac{\lambda_1}{\lambda}\right)\right\} \qquad (2)$$

where G_0 is the shear modulus of the virgin material. The shear modulus G in Fig. 2 (corresponding to a single network situation, i.e, $\lambda_1 = 1$) can be expressed as:

$$G = G_0(1 - f'_{mod} + f'_{xl}) = G_0(1 - f_{mod} + f_{xl}). \quad (3)$$

The linear behavior of Fig. 2 can be expressed by the relation:

$$\Delta f_{xl} = f_{xl} - f_{mod} = f'_{xl} - f'_{mod} = C_0 D, \quad (4)$$

where Δf_{xl} is the net increase in cross-link density, and the constant $C_0 \sim 0.054$ (Mrad)$^{-1}$. Eq. (4) is in good quantitative agreement with recent solvent swelling data on the same material [4]. Eq. (2) solved for $\sigma(\lambda) = 0$ yields the following expression for recovered length λ_s:

$$\lambda_s = \left\{ \frac{1 + f_{eff}\,\lambda_1}{1 + f_{eff}/\lambda_1^2} \right\}^{1/3}, \quad (5)$$

where $f_{eff} = f'_{xl}/(1-f'_{mod})$. Eq. (5) can be inverted to solve for f_{eff} for every experimental value of λ_s in Fig. 3. This yields the values displayed as symbols in Fig. 4 (top), which shows that the dependence of f_{eff} on λ_1 is weak and non-systematic. It is thus natural to construct a model in which f_{eff} is a function of D only (solid curve in Fig. 4 (top)), from which one can solve for the effective fractions of new cross-links f'_{xl} and of modified original chains f'_{mod}, as displayed in Fig. 4 (bottom).

It is interesting to consider the small D limit (5 Mrad or lower) where the transfer function Φ is small and the effective fractions f'_{xl} and f'_{mod} are almost equal to f_{xl} and f_{mod} respectively. In this region we observe linear behavior: $f_{xl} \sim C_{xl}D$ and $f_{mod} \sim C_{mod}D$, where $C_{xl} = 0.114$ and $C_{mod} = 0.060$ Mrad^{-1} respectively. Let us try to interpret this in terms of molecular-level cross-linking and chain scission events. Under cross-linking the number of new chain segments is exactly *twice* the number of original chain segments that get modified, i.e., either two original chain segments cross-link into four new segments (*fourfold-connected* cross-links), or one original segment get cross-linked to a filler surface somewhere in the middle leading to two new segments. On the other hand, chain scission leads to mobile – often volatile small-chain or molecular fragments, or to dangling bonds that can either (i) remain dangling or form a loop onto itself, or reconnect: (ii) to a different dangling bond; (iii) to a filler surface; or (iv) to another chain segment somewhere in the middle (*threefold-connected* cross-links). Processes (iii) and (iv) lead to new chain segments twice that of the originally modified segments, processes (ii) yields the *same* number of segments as the original (i.e. no *net* change in the total number of cross-links), while processes (i) lead to a *decrease* in the net number of cross-links. *The fact that the ratio $C_{xl}/C_{mod} = 0.114/0.060$ is close to 2 indicates that scission events of type (i) and (ii) are rare at low radiation dosages*.

We can show that the behavior of f'_{mod} as shown in Fig. 4 (bottom) can be derived from the assumption that any monomer in the system has the same probability of modification (cross-linking or scission). For simplicity we consider the case of $\lambda_1 = 1$ (i.e. single network) where $f'_{mod} = f_{mod}$. We need to recognize that not all chains are of the same length, but rather the chain length between cross-links, henceforth expressed in terms of the number of

monomers p, follows a statistical distribution, i.e. the MWD. Let $\tilde{n}(p, D)$ be the number of chain segments of length p monomers between cross-links for a sample exposed to a cumulative radiation dosage D. Thus the total number of monomers N in the system, (which is independent of D), and the average chain length $p_{av}(D)$ are respectively given by:

$$N = \sum_p p\tilde{n}(p, D) \quad \text{and} \quad p_{av}(D) = N / \sum_p n(p, D) \qquad (6)$$

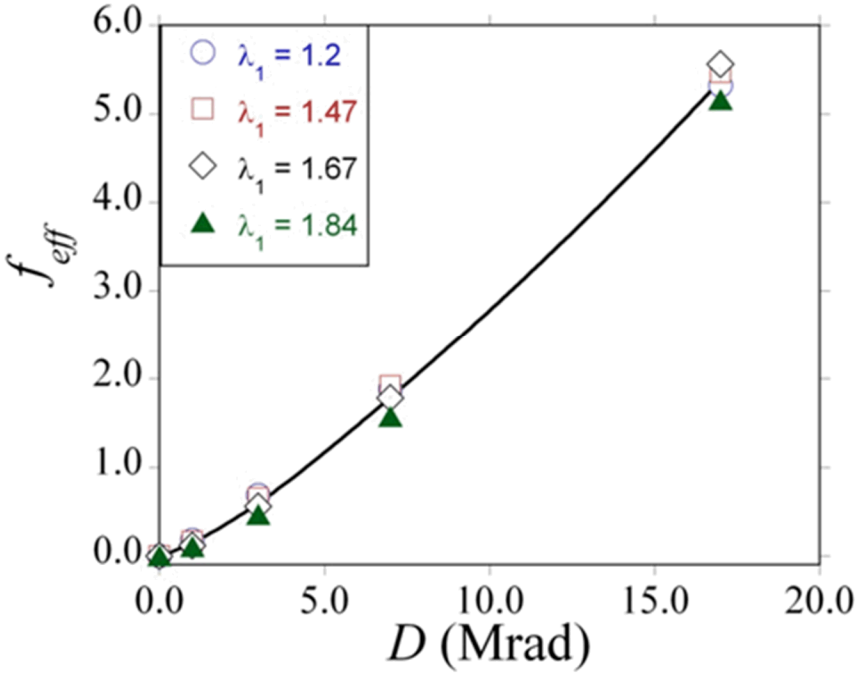

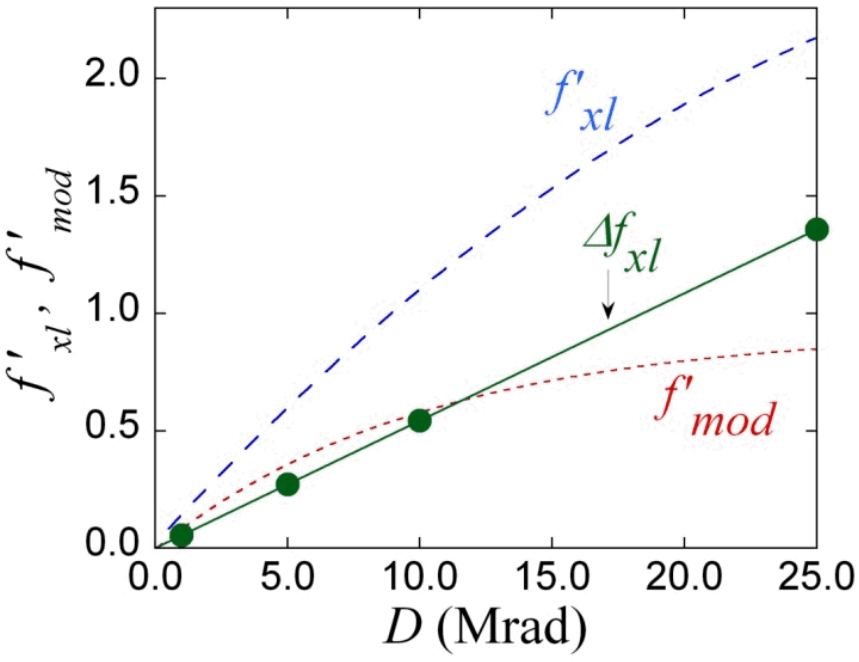

Figure 4. (top) Values of $f_{eff} = f'_{xl}/(1-f'_{mod})$ from the λ_s data using eq. (5), showing weak dependence on λ_1; solid line is the best (λ_1-independent) fit as a function of radiation dosage (D); (bottom) Effective fractions f'_{xl} , f'_{mod} , and $\Delta f_{xl} = f'_{xl} - f'_{mod}$ plotted separately. See text for the definitions of various symbols.

Assuming a constant rate of modification r_{mod} per monomer per unit radiation dosage the probability that an original chain of length p has been modified after exposure to a (cumulative) radiation dosage D is $1 - \exp(-r_{mod}\, pD)$. This yields the following expression for f_{mod}:

$$f_{\mathrm{mod}} = \sum_p [1 - \exp(-r_{\mathrm{mod}}\, pD)]\tilde{n}(p,0) / \sum_p \tilde{n}(p,0) \quad . \qquad (7)$$

For small D, expanding the exponential in eq. (7) yields $f_{mod} \approx r_{mod} p_{av}(0) D$, where $p_{av}(0)$ is the average chain length between cross-links for the virgin material. Thus, $r_{mod} p_{av}(0) = C_{mod} \sim 0.060$ Mrad^{-1}. Using this result in eq. (6) along with the experimentally determined MWD for the virgin material (see below) yields a curve of f_{mod} in excellent agreement with Fig. 4 (bottom).

Molecular Weight Distribution (MWD) between cross-links

^{1}H Multi-Quantum NMR measurements and mesoscale network models

In order to experimentally determine the MWD between junctions/restraints, we utilized the technique of ^{1}H multi-quantum NMR (MQ-NMR) [5], which allows for the quantification of dipolar couplings between protons not averaged to zero due to rapid, but anisotropic motion of the polymer chains. The anisotropic dynamics are due to physical and chemical restrains (due to cross-links and entanglements, respectively). Recent work [6, 7] has established that MQ-NMR based quantification of the residual dipolar couplings in silicone elastomers is very robust, with the following relationship between the residual dipolar coupling (Ω_d) and the number of statistical segments between crosslinks (p):

$$\frac{<\Omega_d>}{<\Omega_0>} = < P_2(\cos\alpha) > \frac{3r^2}{5p}\,, \qquad (8)$$

where $< >$ denotes averaging over all chain orientations, Ω_0 is the dipolar coupling in the absence of motion (pre-averaged by the fast motion of the methyl group), P_2 is the second-order Legendre polynomial, α is the angle between the dipolar vector and the chain axis (i.e., the angle between the backbone chain axis and the Si-C vector), and r is the length of the end-to-end vector, $|\mathbf{R}|$, expressed as a ratio to that of the unperturbed melt, $|\mathbf{R}_0|$, *i.e.*, $r = |\mathbf{R}|/|\mathbf{R}_0|$. Taking the number of monomers in a statistical segment to be 5.7 [8], the distribution $\tilde{n}(p, D)$ can be determined from MQ-NMR measurements using eq. (7). Fig. 5 displays the MQ-NMR spectra for the virgin material as well as for samples exposed to various radiation dosages. The intensity (y-axis) is proportional to the number of monomers in each chain-segment, i.e., $p\,\tilde{n}(p, D)$. Thus the area under each curve is proportional to N, the total number of monomers in the system. It is convenient to define a normalized MWD $n(p, D) = \tilde{n}(p, D)/N$, such that a normalized NMR intensity is equal to $pn(p, D)$, and the total area under each curve is 1. All curves in Fig. 5 (i.e. for each D) are normalized in this way.

The distribution in Fig. 5 represents the main MWD within the pure polymer part. In addition we also see a much weaker peak at smaller chain lengths ($p < 20$) that is likely associated with the silica fillers and/or resins inherent in the TR-55 formulation. Weak dipolar coupling at frequencies above 80 Hz can lead to significant uncertainties in the values of $n(p, D)$ at large values of p (> 300 or so), thus leading to uncertainty in the peak *heights* (especially for $D \sim$ 10 Mrad or below). However, the peak *positions* are robust, as we verified through multiple measurements. Fig. 5 displays a monotonic shift of the MWD to smaller chain lengths and gradual narrowing of the peak as a function of increasing radiation. More specifically, with increasing D the average chain length $p_{av}(D)$ decreases such that the cross-link density $\Delta f_{xl} = p_{av}(0)/p_{av}(D) - 1$ increases linearly in a manner quantitatively consistent with eq. (4) (see Fig. 5 inset) [9].

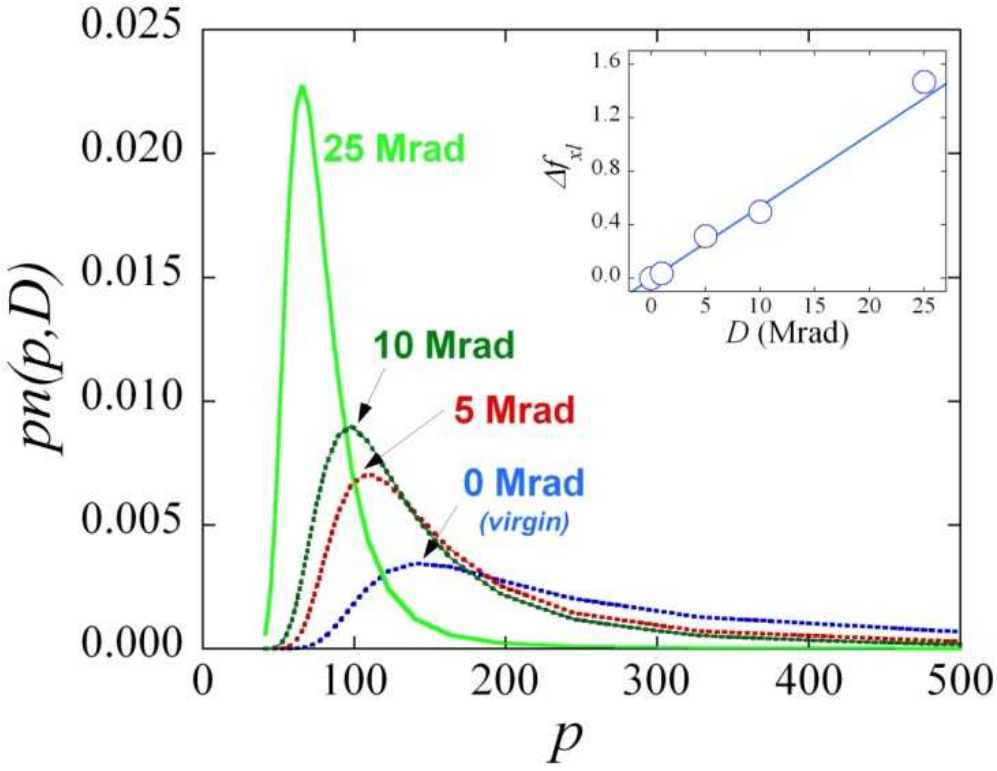

Figure 5. MWD ($pn(p,D)$) from MQ-NMR measurements for various radiation dosages. Inset: Corresponding chain density increment: $\Delta f_{xl} = p_{av}(0)/p_{av}(D) - 1$ as a function of D; solid curve: $y = C_0 D$, see eq. (4).

The above analysis does not identify the type of chemistry prevalent during radiation exposure: is it primarily the formation of new crosslinks, or is it chain scission followed by crosslink formation? How would the results depend on the network functionality, i.e., three-fold or four-fold junctions? Fig. 6 schematically shows possible crosslinking and chain scission processes in a filled rubber that can be brought about by the energetic γ radiation. According to this schematic, except in the case of dangling bond formation, one should have $f_{xl}/f_{mod} \sim 2$. Thus, a value of $f_{xl}/f_{mod} \sim 1.9$ (as obtained above) indicates only a few percent of dangling bonds, but do not provide an indication of which of the various processes (in Fig. 6) dominate. To address this question, the MWD results of Fig. 5 needed to be mimicked through simulations. Two different approaches were taken: (1) a coarse-grained mesoscale simulation approach [10] and (2) a statistical approach involving the population balance of chain lengths of crosslink

segments [11].

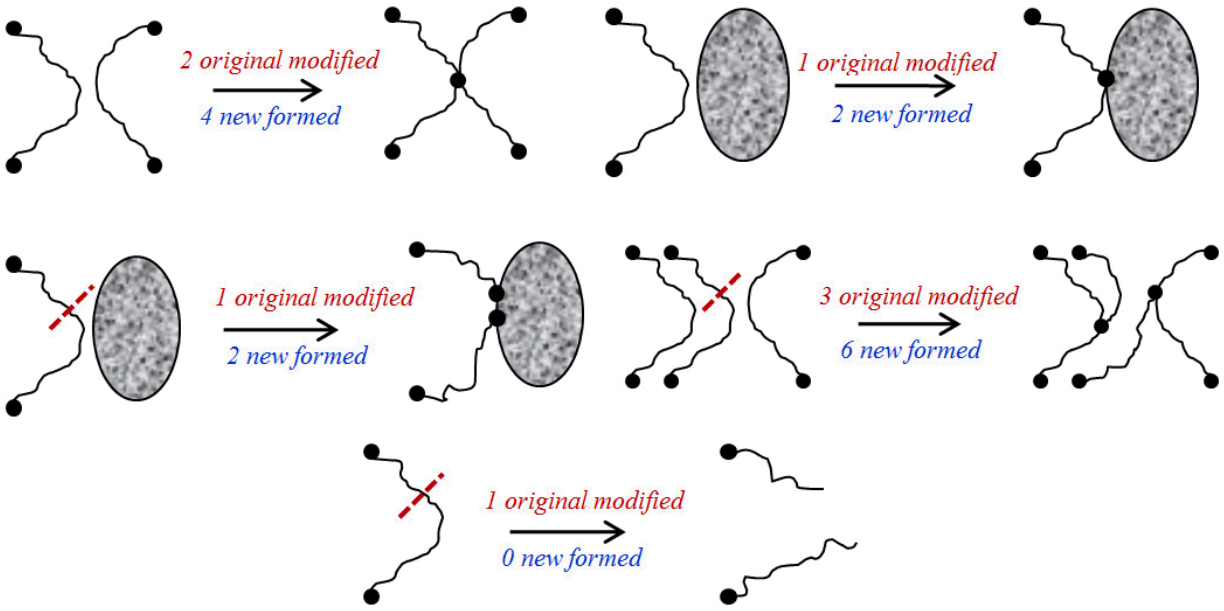

Figure 6. A schematic of how original chain modification and new crosslink formation can occur as a result of radiation-induced processes involving crosslinking (top two figures) and chain scission (bottom three figures). In all cases $f_{xl}/f_{mod} = 2$ except in the case where dangling chains form (bottom figure).

Mesoscale network model:

To simulate the above radiation-induced evolution of MWD, and more specifically to decipher the dominant underlying molecular-level changes in the network, we employed a coarse-grained, mesoscopic polymer network model that has been previously applied to a similar PDMS material [10]. The model consists of a set of cross-link nodes (i.e. junctions) connected via single finite extensible nonlinear elastic (FENE) bonds (that can be potentially cross-linked and/or scissioned), which represent the chain-segments between cross-links. In addition, there is a repulsive Lennard-Jones interaction between all cross-link positions to simulate volume exclusion effects. Since we are only concerned with the polymer network, the filler particles are not explicitly incorporated into the model.

$$V_{FENE}(r) = -\frac{1}{2}kR_0^2 \ln\left[1-\left(\frac{r}{R_0}\right)^2\right], \quad r < R_0 \tag{9}$$

$$V_{LJ}(r) = \begin{cases} 4\epsilon\left[\left(\frac{\sigma}{r}\right)^{12} - \left(\frac{\sigma}{r}\right)^{6}\right] + \epsilon, & r \le 2^{1/6}\sigma \\ 0, & r > 2^{1/6}\sigma \end{cases} \tag{10}$$

The first step was to create a network that resembles the virgin distribution of Fig. 5. To this end, we placed more than 4000 random "nodes" (representing junctions) in a 3-D cubic box with periodic boundary conditions. Pairs of junctions within a chosen cut-off were then randomly connected by FENE bonds. The Lennard-Jones and

FENE interaction parameters were adjusted and the degree of polymerization (p) for a given length of a FENE bond calibrated until the MWD computed from our network matched the experimental MWD of the virgin material.

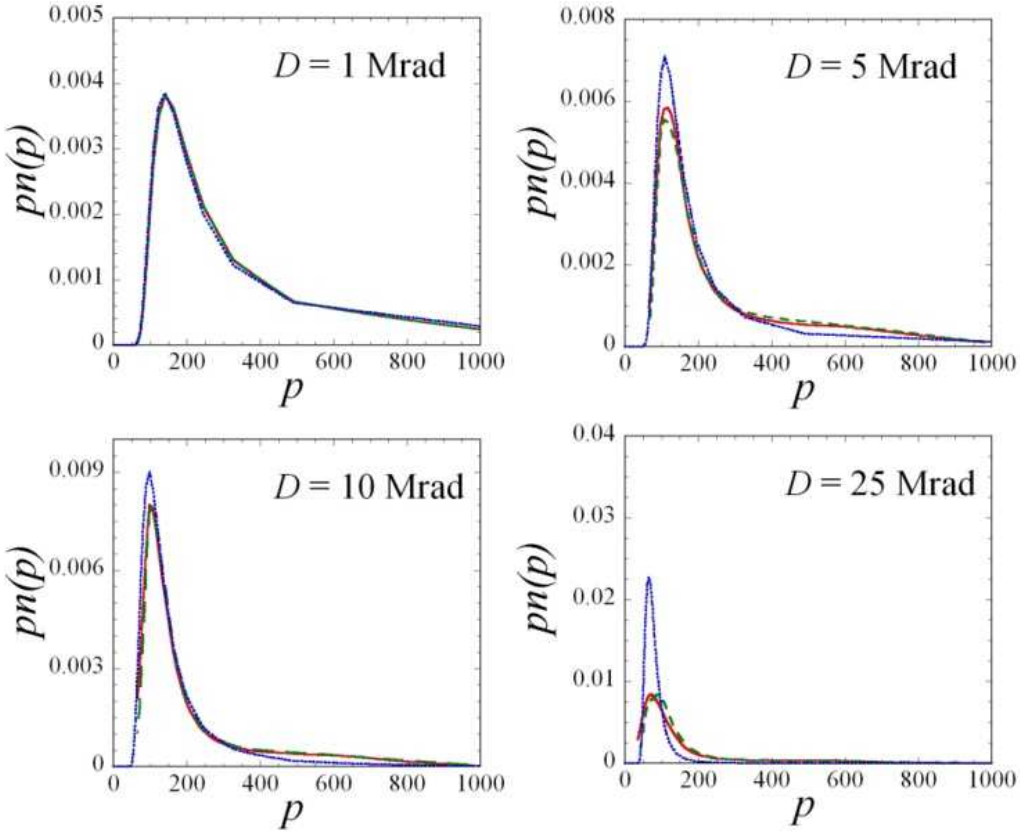

Figure 7. Comparison of experimental MWD of Fig. 5 (blue line) with computed MWD for fourfold-linking only (red solid line) and threefold-linking only (green dashed line).

To simulate the radiation-induced evolution of the above network, we first considered the situation with only cross-linking and no scissioning (i.e. only fourfold-connections). For this, we created the virgin network with only fourfold-connected junctions, and performed additional random cross-link operations between FENE bonds (i.e. segments) in accordance with Δf_{xl} values given by eq. (4). We added new cross-links in radiation dosage steps of 1 Mrad, and at each step structurally optimized (i.e. relaxed) the new network using the LAMMPS code [12].

Fig. 7 displays the simulated evolution of MWD of the above network (red curve) under fourfold-coordination for four different radiation dosages along with the experimental data (blue line). We also considered the MWD evolution when all new cross-links were threefold-connected (i.e. scission-induced), as shown by green dashed lines. The differences in MWD between fourfold and three-fold connected cases are negligible, and both mechanisms lead to excellent agreement in the peak positions as compared to NMR data. The differences between peak heights, especially for $D \leq 10$ Mrad are not surprising given the uncertainty in the NMR data in the long-tail part (see discussion above Fig. 5). However at 25 Mrad, the disagreement between the experimental and simulated data is significant and point to effects not considered in the simulations. To explain such differences, we performed

simulations in which we allowed for the presence of dangling bonds (and/or loops) which did not form junctions. This leads to simulated peaks to be narrower and higher, closer to the NMR data. Similar effects could also be expected from the creation of volatile small-chain fragments.

Population balance model:

Finally, Dinh et al.[113] carried out a statistical analysis of the distribution of crosslink segment lengths and its evolution with network changes brought about by irradiation. The basic idea starts from the fact that when two chains of lengths p and q crosslink somewhere in the middle, it forms four chains of lengths $p - m$, m, $q - n$, and n (where $m < p$ and $n < q$). The evolution of the MWD, i.e., the frequency distribution of chains of different lengths is governed by the probabilities of different types of chemical processes caused by radiation, i.e., crosslinking, chain scissioning, loop formation, etc. It also depends upon the details of the type of crosslinking process, e.g., H-linking or Y-linking or a mixture of both.

Such a method of tracking the distribution of chain lengths, known as population balance (PB) was first applied by Saito [13] to a set of initially free (i.e. non-crosslinked) polymer chains, while Dinh at al. [11] derived the PB equations appropriate for a system of crosslinked chains. The MQ-NMR MWD data on the virgin material was used to create a starting population of crosslink lengths, which was evolved according to various crosslinking and scissioning schemes. The hope was that by matching the simulated MWD evolution to the MQ-NMR data as a function of radiation one would be able to identify the dominant crosslinking scheme. Unfortunately, the PB-simulated MWD corresponding to several different crosslinking schemes were nearly identical, and agreement with the MQ-NMR was only qualitative in nature. Nonetheless, the work was able to put bounds on various rates of these processes and further confirmed that a competition of these phenomena determines the overall evolution of the effect of irradiation. More details can be found in ref. [11].

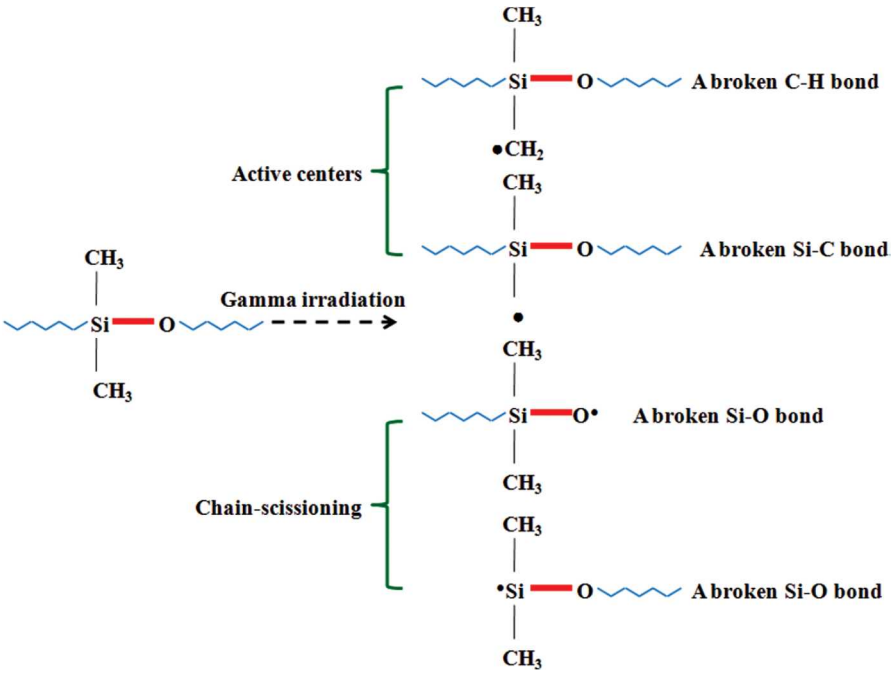

Figure 8. Cartoons depicting active centers and chain-scissioning formed under γ-radiation.

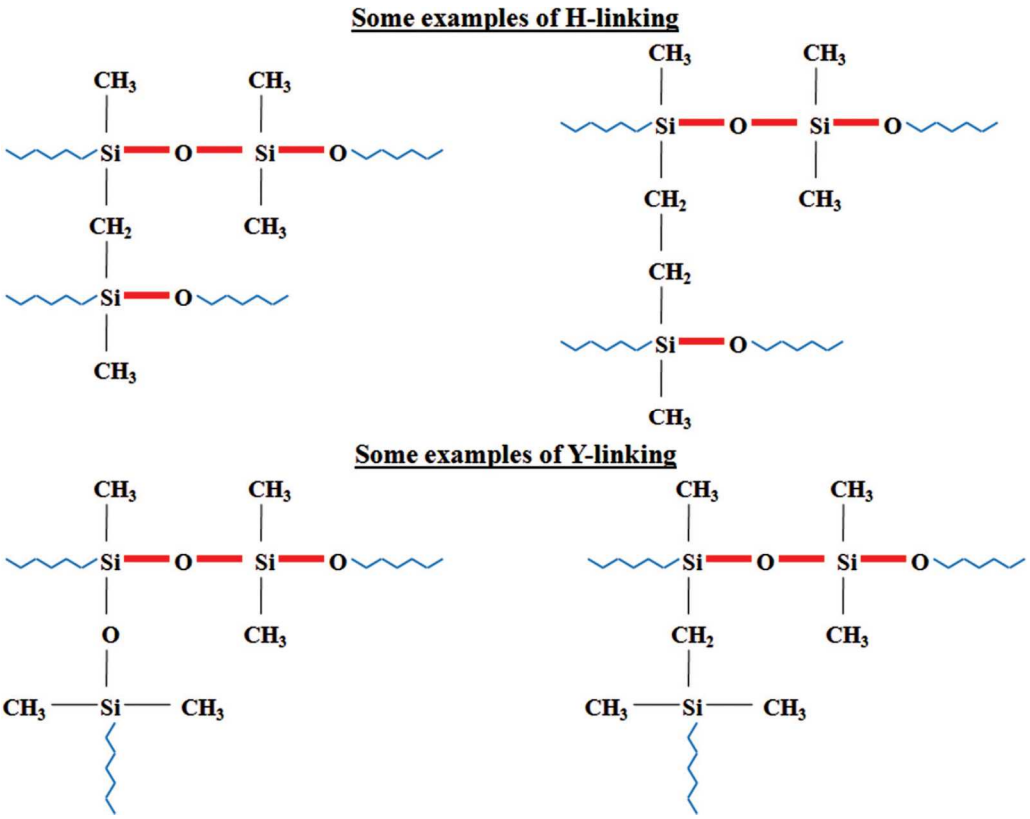

Figure 9. A schematic of possible structures formed via H-linking and Y-linking.

Combined modeling of radiation hardening and Mullins softening

Mechanical measurements (Permanent Set):

All experiments were performed on the commercial silicone elastomer TR-55 from Dow Corning. Thin rectangular samples were stretched to specific strain levels and exposed to controlled dosages of γ-radiation from a Co-60 source (1.4MeV, ~ 0.1 Mrad/hour dose rate) in a non-reactive nitrogen atmosphere. Seven different strain levels were studied, corresponding to stretch ratios λ_1 = 1.20, 1.47, 1.67, 1.84, 2.00, 2.33, 2.67. Following exposure to controlled duration (and therefore dosages) of radiation, each sample was removed from the irradiation chamber, released from the λ_1-strain, and allowed to relax at ambient conditions for 24 hours. The relaxed samples were then subjected to measurement of the new equilibrium length, called the recovered length λ_s. After several weeks of further equilibration, stress-strain analysis was carried out for 5 load/unload cycles at strains of up to 50% elongation. The stress-strain analysis was performed on rectangular specimens (width ~ 3 mm and thickness 0.6-0.9 mm) using a Instron 5565 dual-column electromechanical test system with an initial grip separation of ~ 20 mm and a stretching rate of 20 mm/min.

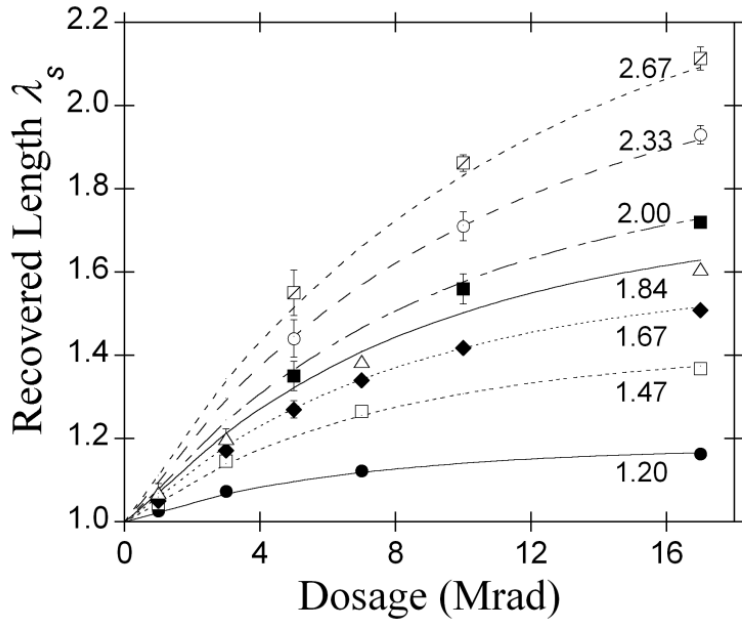

Figure 10. Recovered length (λ_s) as a function of radiation dosage for different values of tensile stretch ratios (λ_1) at which the material is subjected to radiation. The symbols denote experimental measurements while the lines (solid, dashed, and dotted) are theoretical results using λ_1-independent f_{eff} (see text). The λ_1 values are indicated by each curve.

Fig. 10 plots the measured recovered length (λ_s) as a function of radiation dosage D for the different values of λ_1. Error bars indicate sample-to-sample variation in cases where multi-sample measurements were performed. A subset of these results was reported previously [9], and were quantitatively interpreted using Tobolsky's 2-stage independent network model [1]. Fig. 11 plots a typical stress-strain response of such samples (only the loading curves are shown and the unloading curves hidden for clarity). The main feature is that there is strong dependence on the cycle number. In particular, in cycle 1 the response is much steeper, corresponding to a significantly higher elastic modulus, while the response becomes progressively softer in subsequent cycles, but with a much smaller drop-off than between cycle 1 and cycle 2. This type of softening has long been known to occur in filled rubber materials and is generally known as the Mullins effect [15]. At the end of cycle 1 a small permanent stretch (~ 2%) is also incurred, which is smaller than typical permanent sets reported in Fig. 10. It is important to note here that the recovered length in Fig. 10 was obtained *prior* to subjecting the samples to the stress-strain cycles as in Fig. 11.

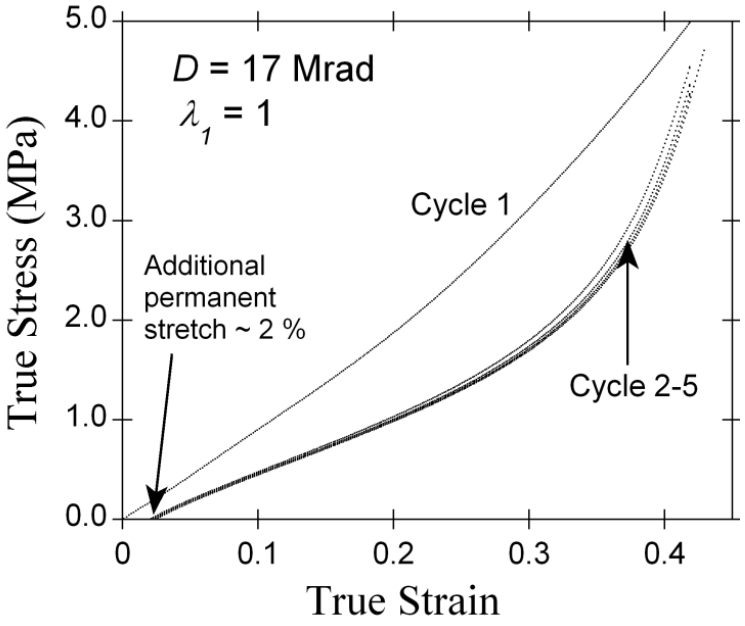

Figure 11. Typical stress-strain response of a radiation-exposed TR-55 sample through the first five cycles. The data shown corresponds to a sample that was exposed to 17 Mrad of radiation (under $\lambda_1 = 1$) and then stretched to a maximum of 50% of its original length during each cycle.

Next the Young's modulus (E) was extracted from the stress-strain *slope* at small deformation (corresponding to strain levels of 5% or less) for various cycles and various values of λ_1 and D. Fig. 12 displays the results for E in cycles 1 and 5. We observe the following trends: (1) for all values of λ_1 the modulus increases as a function of D within each cycle. For $\lambda_1 = 1$ and cycle 1 this increase is nearly linear, as observed previously [9]; (2) for all values of λ_1 and D the modulus significantly decreases from cycle 1 to cycle 5, similar to the softening behavior seen in Fig. 11. The decrease in modulus is the largest for $\lambda_1 = 1$ and gets progressively smaller for increasing values of λ_1; (3) as a function of λ_1 the modulus displays complex behavior that can be increasing, decreasing, or non-monotonic depending upon the cycle and the radiation dosage D. In particular, in cycle 1 the modulus E shows an overall decreasing trend as a function of increasing λ_1, with the rate of decrease $|\partial E/\partial \lambda_1|$ getting smaller with increasing λ_1 and increasing D. In cycle 5 on the other hand E shows more complex behavior as a function of λ_1, decreasing at D = 5 Mrad, increasing at D = 17 Mrad, and non-monotonic at intermediate values (10 Mrad). The above behavior of E can be traced to a combination of two effects: (i) material softening due to the Mullins effect; and (ii) radiation hardening of the elastomer due to the creation of a net number of new cross-links. In the following we analyze the above results within the framework of Tobolsky's 2-stage network theory using a simple constitutive materials model for the mechanical response of incompressible rubber.

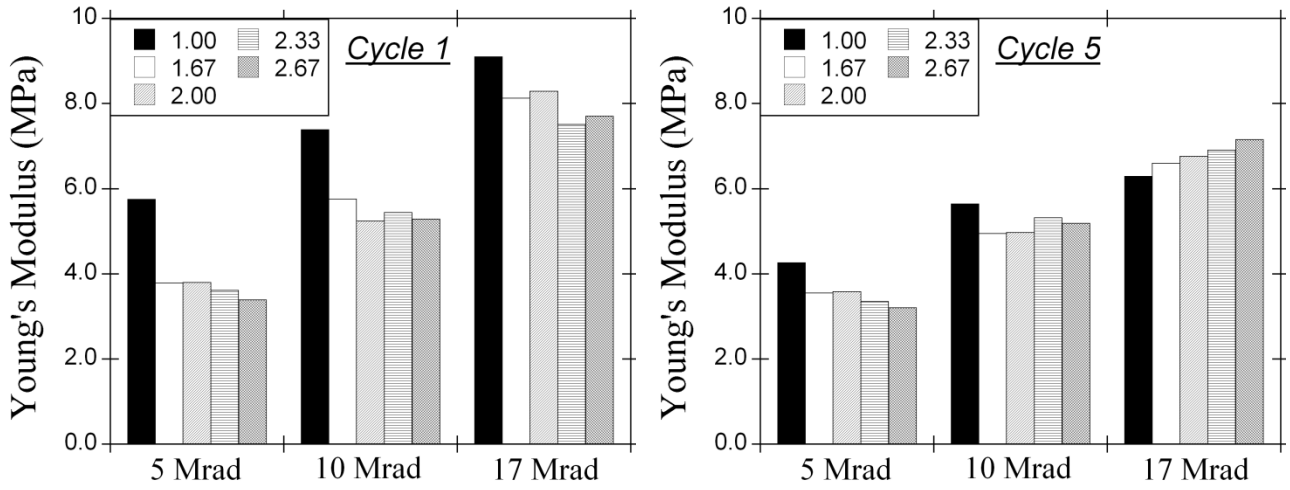

Figure 12. Young's modulus obtained from the small-deformation slope of experimental stress-strain data for various values of λ_1, three different radiation levels, and two cycles (cycle 1 and cycle 5). Depending on the cycle and the radiation level the elastic modulus displays increasing, decreasing, and non-monotonic behavior as a function of λ_1.

Constitutive Model:

To analyze the experimental data on recovered length λ_s (Fig. 10) and Young's modulus E (Fig. 12) we adopted the Neohookean stress response model (eq. (1)). Before deriving a general formula for the Young's modulus E we note that for the special case $\lambda_1 = 1$ the Young's modulus is simply three times the shear modulus, i.e., $E = 3G$. Thus the near-linear increase of E with D for λ_1=1 in cycle 1 (see Fig. 12 (left)) can be expressed as $G = G_0(1+C_0D)$,

where $G_0 \sim 1.5$ MPa is the shear modulus of the pristine material, D the radiation dosage in Mrad, and C_0 is a constant ~ 0.05 Mrad^{-1}. This change in modulus results from a net increase in the number of cross-links in the system induced by radiation.

First we inverted eq. (5) to obtain the following expression for f_{eff} (previously defined as $f'_{xl}/(1-f'_{mod})$):

$$f_{eff} = \frac{\lambda_1^2(\lambda_s^3-1)}{(\lambda_1^3-\lambda_s^3)} \qquad (11)$$

When the experimental values of λ_s and λ_1 (from Fig. 10) are used in eq. (11) we find that f_{eff} is a function of D only, and nearly independent of λ_1. The values of f_{eff} (averaged over λ_1) as a function of D is plotted in Fig. 13, with the behavior well-described by the exponential fit (solid line):

$$f_{eff} = \exp(\alpha_1 D - \alpha_2 D^2) - 1 \qquad (12)$$

where constants $\alpha_1 \sim 0.165$ Mrad^{-1} and $\alpha_2 \sim 0.003$ Mrad^{-2} respectively.

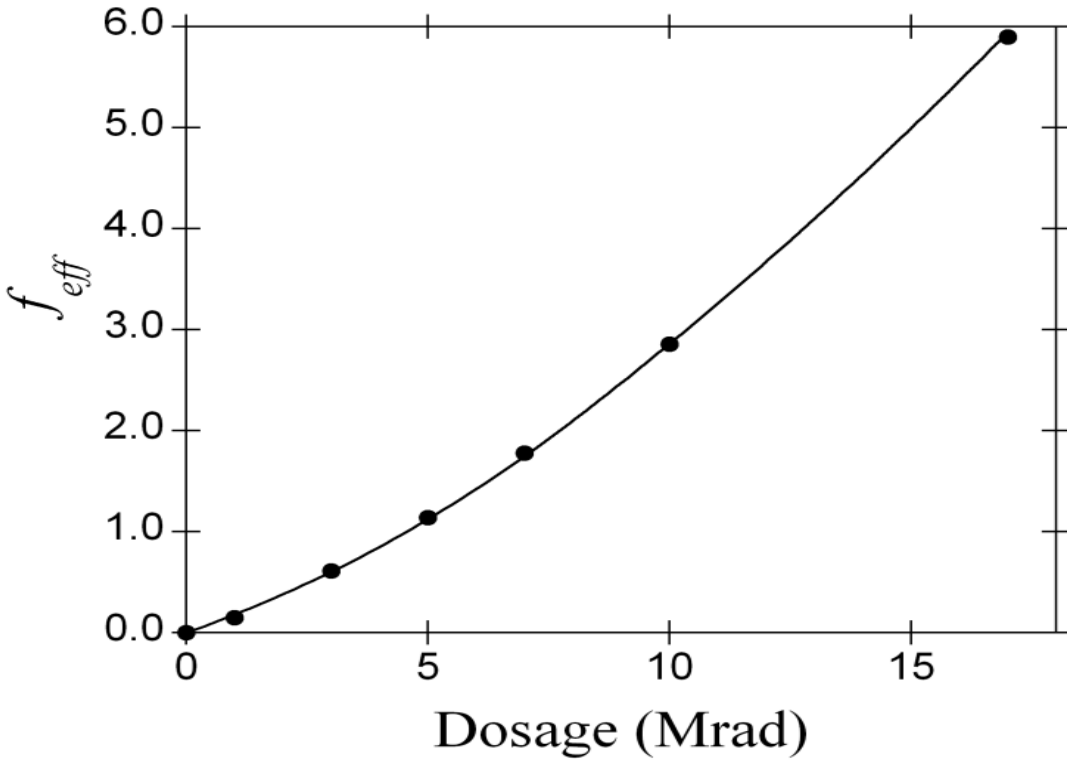

Figure 13. The quantity f_{eff} (see text) as a function of radiation dosage D: the points correspond to (λ_1-averaged) values obtained by inserting experimental recovered lengths (λ_s) into eq. (11), while the solid line corresponds to an exponential fit given by eq. (12).

Next we analyze the modulus E, defined as the small-deformation stress-strain slope about the altered equilibrium (λ_s) is given by:

$$E = \lim_{\varepsilon \to 0} \frac{\sigma(\lambda_s(1+\varepsilon)) - \sigma(\lambda_s)}{\varepsilon} = \left(\frac{\partial \sigma}{\partial \lambda}\right)_{\lambda_s} \lambda_s , \qquad (13)$$

where ε is the uniaxial deformation strain. Eqs. (1), (2), (3) and (6) yield (after some algebraic manipulation) the following expression for E:

$$E = G_0 \frac{(1+C_0 D)}{(1+f_{eff})}\left[\left(2\lambda_s^2 + \frac{1}{\lambda_s}\right) + f_{eff}\left(2\frac{\lambda_s^2}{\lambda_1^2} + \frac{\lambda_1}{\lambda_s}\right)\right] \qquad (14)$$

For $\lambda_1 = 1$ there is no permanent set, i.e., $\lambda_s = 1$, which when substituted in eq. (14) yields the simple relation $E = 3G_0(1+C_0D) = 3G$, as mentioned before. Assuming a constant $G_0 \sim 1.5$ MPa in eq. (14) one obtains an increasing E as a function of increasing λ_1 as shown in Fig. 14, a behavior in clear disagreement with the experimental pattern of Fig. 12.

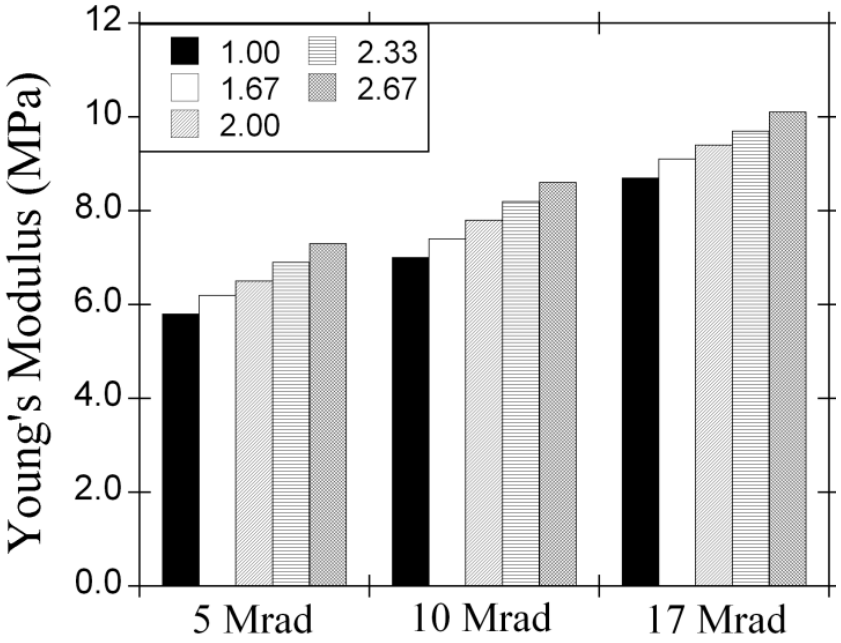

Figure 14. Young's modulus (E) as predicted from eq. (7) with a constant G_0 (= 1.5 MPa) independent of stress-strain cycling.

The behavior in Fig. 14 arises under the assumption that G_0 is constant and independent of the cycle number, λ_1, and D. This is equivalent to the assumption that the rubber network does not have any hysteresis effects, i.e., no Mullins effect. This assumption is clearly not correct for the experimental TR-55 samples as evidenced from the softening in Fig. 11 with strain cycling. In fact Figs. 11 and 12 indicate two different stages at which the material softening takes place: (1) during the several-week-long annealing period following the λ_s measurements. This softening happens only for $\lambda_s > 1$, with the amount of softening increasing with increasing λ_s (and therefore increasing λ_1); (2) during the first stress-strain cycle following the annealing period. The amount of this softening decreases with increasing λ_1. The first type of softening leads to the behavior of E as seen in Fig. 12 (left), while the second type of softening causes the change from the behavior in Fig. 12 (left) to that in Fig. 12 (right). We elaborate on this point in the discussion below.

Although the Mullins effect has been known for several decades, the underlying microscopic driving force is still unclear [16]. Suggestions range from the cleavage of chemical bonds between rubber and filler, slipping and disentanglement of chains, rupture of filler clusters, and so on. The true mechanism notwithstanding, it is clear that any of these processes will lead to a decrease in the overall cross-link density. In addition, the propensity for each of these processes is expected to: (1) increase with the stress level the material is subjected to; and (2) decrease with increasing radiation dosage. The latter creates additional cross-links that reduce the average stress levels per cross-link for a given strain level. As a simple model illustrating these two effects on the cycle 1 response we have explored the behavior of E when the pristine shear modulus G_0 in eq. (14) is rescaled by a multiplicative factor, i.e.,

$$G_0 \rightarrow G_0[1-\alpha(\lambda_s-1)], \qquad (15)$$

where α is a decreasing function of the radiation dosage D. Fig. 15 plots the resulting values of E for the parameter values of $\alpha = 0.95$, 0.48, and 0.19 for $D = 5$, 10, and 17 Mrad respectively. This behavior is quantitatively consistent with Fig. 12(left).

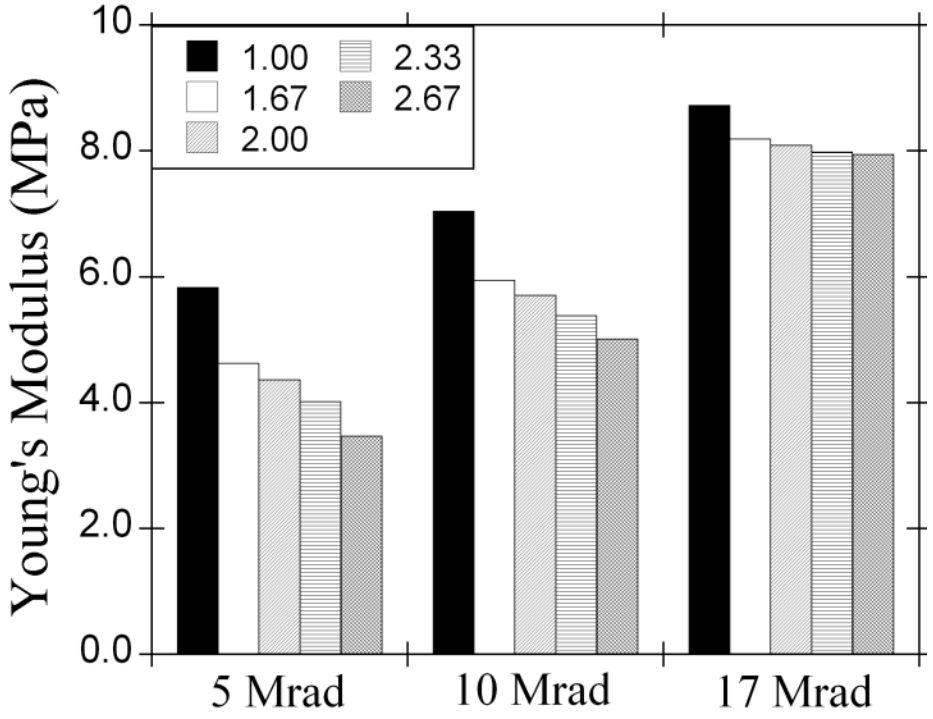

Figure 15. Young's modulus (E) in cycle 1 as predicted from eq. (14) by rescaling the pristine shear modulus G_0 (= 1.5 MPa) with a multiplicative factor $[1-\alpha(\lambda_s-1)]$. This factor represents a simple model that illustrates the effect of λ_s and radiation dosage D on the cycle 1 response. See text.

Finally, the behavior of E in cycle 5 (Fig. 12(right)) can be interpreted as follows. With repeated cycling further loss in cross-links continues to occur until all the loose links (weak chemical bonds to fillers or physical entanglements) are removed from the system. For larger values of λ_1 (and resulting larger λ_s) a larger fraction of these links are removed during the several-week-long annealing period (i.e. before the first stress-strain cycle), which is consistent with a higher degree of softening and a decreasing E with increasing λ_1 in cycle 1. As a

consequence, any additional softening in subsequent cycles is higher for smaller values of λ_1. This effect, in conjunction with a decreasing $|\partial E/\partial \lambda_1|$ with increasing D in cycle 1 (see Fig. 12(left) or Fig. 15) leads to less negative values of $\partial E/\partial \lambda_1$ in cycle 5 (as compared to cycle 1), which can even become positive for large D (as seen in Fig. 12(right) for D = 17 Mrad).

Eq. (15) was the first model [14] we built that incorporates Mullins softening. Recently, we have constructed a more complex model to describe the behavior of SE1700 rubber (used as ink to create additively manufactured foam) under similar experiments as discussed above for TR-55. The model consists of modifying eq. (14) as follows (written in terms of stress σ):

$$\sigma = G_0 \frac{(1+C_0 D)}{(1+f_{eff})} \frac{1}{f_M} \left[\left(\lambda'^2 - \frac{1}{\lambda'} \right) + f_{eff} \left(\lambda''^2 - \frac{1}{\lambda''} \right) \right] \quad , \qquad (16)$$

where λ' and λ'' are the uniaxial stretch ratios in the original and newly formed networks, respectively, and f_M is an additional function that incorporates Mullins softening. In the current model, the uniaxial stretch ratios are given by:

$$\lambda' = \frac{\lambda}{1+C_1(\lambda_1 - 1)} \quad ; \quad \lambda'' = \frac{\lambda'}{\lambda_1} \quad , \qquad (17)$$

and the f_M factor is of the form:

$$f_M = 1 + C_2(\lambda_1 - 1) \qquad (18)$$

The current parameters of the above model have been developed for the SE1700 rubber. However, we believe that with simple re-parameterization this model can be adapted to TR-55 as well.

APPENDIX I: A phenomenological constitutive model to understand Mullins effect

Background: Modulus softening and permanent set in filled polymeric materials due to cyclic loading and unloading, commonly known as the Mullins effect, can have a significant impact on their use as support cushions. A quantitative analysis of such behavior is essential to ensure the effectiveness of such materials in long-term deployment. In FY12-13 we combined existing ideas of filler-induced modulus enhancement, strain amplification, and irreversible deformation within a simple non-Gaussian constitutive model to quantitatively interpret recent measurements on a relevant PDMS-based elastomeric cushion (TR-55) relevant to stockpile. We find that the experimental stress-strain data is consistent with the picture that during stretching (loading) two effects take place simultaneously: (1) the physical constraints (entanglements) initially present in the polymer network get dis-entangled, thus leading to a gradual decrease in the effective cross-link density, and (2) the effective filler volume fraction gradually decreases with increasing strain due to the irreversible pulling out of an initially occluded volume of the soft polymer domain.

The Mullins effect [15, 16] typically has the following characteristic signatures: (1) significant softening results upon the first unloading cycle; (2) the amount of softening increases with increase in the maximum strain in the first cycle; (3) subsequent loading closely follows the first unloading curve and the unloading shows much less softening as long as the previous maximum strain is not exceeded; (4) if a subsequent loading exceeds the previous maximum, it acts as if to follow a continuation of the previous maximum loading curve; (5) there can be an induced anisotropy even in rubber that is isotropic in its virgin state; and (6) there is often a small but noticeable permanent set at the end of the first unloading curve. The permanent set typically increases upon unloading from an increased maximum strain, although in some cases it can recover after a long resting time. Although the Mullins effect has been observed in both filled and unfilled rubber, it is particularly pronounced in systems with significant filler content.

Analysis by many groups over the past several decades has led to the suggestion of several different physical mechanisms behind the Mullins effect. Many authors have taken the viewpoint that stiff filler particles lead to an enhanced elastic modulus through rubber-filler attachments that provide additional restrictions on the cross-linked rubber network. Softening results from the breakdown, slippage, or loosening of some of these attachments, a phenomenon commonly referred to as stress softening. Modeling such phenomenon has typically involved the representation of filled rubber with multiple networks, and strain-induced damage or alteration of one of the networks, while more detailed refinements, e.g., that involving the cluster topology of fillers is progressively being introduced. An alternative way to analyze Mullins effect has been to treat filled rubber as a system comprised of soft and hard domains that evolve under stretch – softening is caused by the quasi-irreversible increase in the volume fraction of the soft domain. Models based on the second line of thought postulate a localized non-affine deformation of the molecular networks due to short chains reaching their limits of extensibility, and effective strain amplification in the soft domain as compared to the actually applied strain because of almost zero strain in the hard domain.

The first viewpoint of describing Mullins effect typically necessitates complex materials-based models that

continue to get refined in the current literature. On the other hand, the second viewpoint (i.e. strain amplification) is more phenomenological, and has been shown to be easily implementable in finite-elements simulation codes. However, there is some ambiguity in how strain should be amplified. For instance, Mullins and Tobin [17] suggested amplifying the uniaxial strain, Govindjee and Simo [18] suggested amplifying the total deformation gradient, while Boyce and co-workers [19, 20] have suggested amplifying the first invariant of stretch I_1.

Measurements: The mechanical measurements were performed on rectangular samples (~3 mm wide by ~1 mm thick) of TR-55 that were stretched to a maximum engineering strain of $\varepsilon_{max} \sim 2.15$ at a rate of 20 mm/min under ambient conditions. TR-55 consists of silicone gum stock (primarily PDMS) filled with 30 wt% of fumed silica, which corresponds to a filler volume fraction of ~ 16%. The initial grip separation was 20 mm. After 5 s at ε_{max} the external stretching force was removed and the samples relaxed to a state of equilibrium (i.e., zero stress). After 5 s in the zero stress condition, the samples were stretched again to the previously attained maximum stretch. The cycle was repeated four times. During the fifth loading cycle, the sample was stretched beyond the previous maximum stretch. Fig. A1 plots the stress-strain response. It exhibits many of the characteristic Mullins signatures mentioned above. Two aspects that are most noteworthy are the significant softening and a large permanent set incurred upon the very first unloading, with a recovered engineering strain $\lambda_s - 1 \sim 18\%$. If such strain levels are not accounted for prior to the deployment of the elastomeric component in mechanical support devices, it can have undesired effects in the long-term performance.

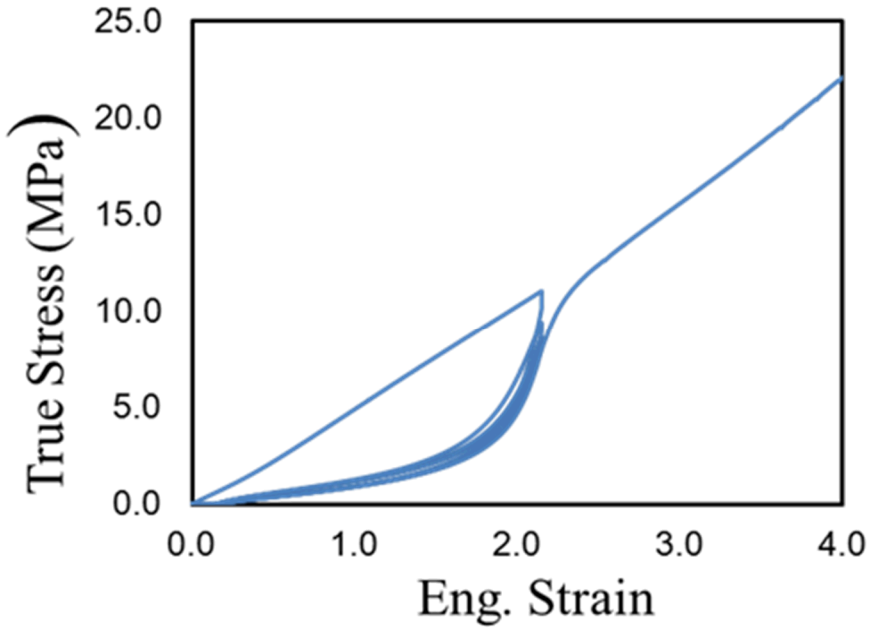

Figure A1. Stress-strain curve for a typical TR-55 sample that underwent five loading and four unloading cycles with the first four loading cycles limited to an engineering strain of 2.15 and the fifth loading cycle exceeding this strain. In addition to the typical Mullins softening, one observes a large permanent set with a recovered engineering strain $\varepsilon_s \sim 18\%$.

Phenomenological Model:

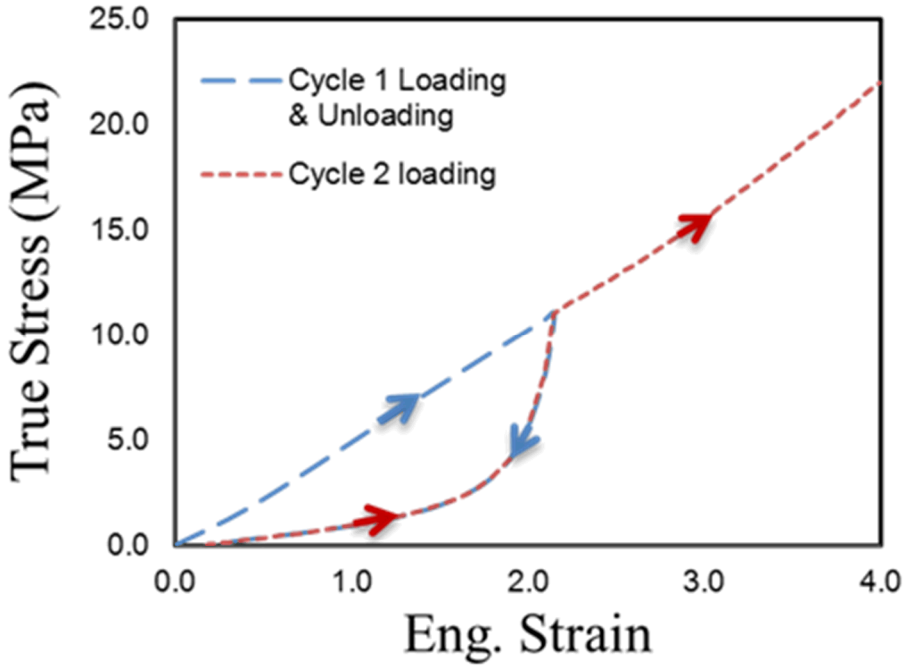

Figure A2. A simplified representation of Fig. A1 for modeling purpose.

Given that the difference between the first unloading curve and subsequent loading and unloading curves are small until the previous maximum strain is exceeded, a common simplification is to ignore such difference, as illustrated in Fig. A2. Thus, a quantitative analysis of the Mullins effect becomes an exercise in describing the first loading and the first unloading curves for varying maximum strain levels. In order to develop an appropriate stress-strain relation, i.e., a materials model, we start from the simple Neohookean model often employed in the description of the mechanical response of unfilled, cross-linked rubber. Under a uniaxial strain, the expression for stress in this model is given by:

$$\sigma(\lambda) = G_0\left(\lambda^2 - \frac{1}{\lambda}\right) \qquad \text{(A1)}$$

where σ is the true stress, λ is the stretch ratio (= $1 + \varepsilon$, ε being the engineering strain), and G_0 the shear modulus. For an unfilled network system G_0 can be expressed as a function of the cross-link density, with some dependence on the network topology, junction coordination, etc. The above model is based on the assumption that the cross-links behave essentially as Gaussian chains, which can be justified under not-too-large strains. Under large strains finite extensibility needs to be taken into account via non-Gaussian statistics, under which eq. (A1) gets modified to the Wang-Guth model [21]:

$$\sigma(\lambda) = \frac{G_0\sqrt{N}}{3}\left\{\lambda\mathcal{L}^{-1}\left(\lambda/\sqrt{N}\right) - \frac{1}{\sqrt{\lambda}}\mathcal{L}^{-1}\left(1/\sqrt{\lambda N}\right)\right\}, \qquad \text{(A2)}$$

where N is a parameter describing the finite chain length of the small-chain cross-links (presumably related to

polymer-filler attachments), and $\mathcal{L}^{-1}$ is the inverse of the Langevin function given by $\mathcal{L}(x) = \coth(x) - 1/x$. In the small strain limit, where $\lambda/\sqrt{N} << 1$ (assuming $N >> 1$), the inverse Langevin function can be approximated as $\mathcal{L}^{-1}(\lambda/\sqrt{N}) \approx 3\,\lambda/\sqrt{N}$, and eq. (A2) reduces to eq. (A1). The Wang-Guth model, eq. (A2), is suitable for describing the mechanical response of networked, elastomeric systems without fillers. For filled systems, Mullins and later workers found it necessary to incorporate the notion of strain amplification. To represent strain amplification we follow the original work of Mullins and Tobin and replace the stretch ratio λ in eq. (A2) by an amplified stretch ratio Λ given by:

$$\Lambda = 1 + X(\lambda - 1) \quad , \qquad \text{(A3)}$$

where X is an amplification factor that depends on the *effective* volume fraction v_{eff} of the hard domain, i.e., fillers. A commonly used form for X as a function of v_{eff} is given by:

$$X = 1 + 3.5v_{eff} + bv_{eff}^2. \qquad \text{(A4)}$$

In eq. (A4) b is a parameter with a commonly used value of 18, which is obtained by comparing with the widely adopted filler-enhancement model due to Guth and Gold that is applicable for well-dispersed nearly spherical filler particles with not-too-high volume fraction (≈ 15 % or below). Replacing the stretch ratio λ in eq. (A2) by Λ, and accounting for the fact that the elastic response comes only from the soft part of the material, we obtain the following materials model for filled rubber:

$$\sigma(\lambda) = (1 - v_{eff})\frac{G_0\sqrt{N}}{3}\left\{\Lambda\mathcal{L}^{-1}(\Lambda/\sqrt{N}) - \frac{1}{\sqrt{\Lambda}}\mathcal{L}^{-1}(1/\sqrt{\Lambda N})\right\}, \qquad \text{(A5)}$$

Eq. (A5) can be used to describe the Mullins effect quantitatively by assuming that during the first loading curve the soft part of the matrix is being pulled out of the hard region thus progressively decreasing the relative volume fraction v_{eff} of the hard domain. The volume fraction of the soft part $(1 - v_{eff})$ should increase monotonically with increase in the maximum strain level, and expected to reach a saturation value depending upon the relative amount of filler particles that was originally mixed into the rubber formulation.

Finally, to account for the observed permanent set (see Fig. A1) the formula for stretch ratio, eq. (3) was modified as follows:

$$\Lambda = 1 + X\left(\frac{\lambda}{\lambda_s} - 1\right), \qquad \text{(A6)}$$

where λ_s is the recovered length, which in our model is assumed to increase linearly with λ during the first loading cycle until a maximum value of $\lambda_{s,max}$ is reached at the maximum strain. During any subsequent unloading and reloading λ_s remains constant at this maximum value until the previously attained maximum strain is exceeded. The numerical value of $\lambda_{s,max}$ is obtained from the experimental recovered length at the end of the first unloading curve. Equations (A4) - (A6) constitute the materials model employed in the simulations presented below.

Results:

In order to compute the stress-strain behavior $\sigma(\lambda)$ using the model developed in the previous section, the parameters G_0, b, N, υ_{eff} and λ_s need to be determined. The motivation of this project was to obtain these parameters (some of which could vary with the applied strain ε if necessary) such that not only is the computed stress in quantitative agreement with that observed experimentally for TR-55 (Fig. A1), but also the parameters conform with previous knowledge about similar filled systems. For instance, given ~ 16% volume fraction of fillers in TR-55, the parameter b is expected to be ~ 18, while the filler-enhancement factor at low-stress should be roughly in the range 2 - 4. From the phantom network model G_0 can be assumed proportional to the cross-link density (ν_{xlink}) through the equation: $G_0 = \nu_{xlink}(1-2/f_c)k_BT$, where f_c is the average network coordination, k_B the Boltzmann constant, and T the absolute temperature. However, there is always a degree of uncertainty as to the nature of the cross-link, e.g., a chemical cross-link vs. a physical entanglement. Swelling experiments on unfilled systems of similar polymeric material indicate that the chemical cross-link density is much too small (by a factor of ~ 4-5) to account for the observed mechanical modulus at low strain. This leads us to believe that prior to being subjected to any strain, the polymer chains in the TR-55 material are strongly entangled, while upon swelling or mechanical stretching a significant fraction of these entanglements become dis-entangled, thus reducing the effective value of G_0.

Fig. A3 (dashed-dotted curve) displays the results of our model calculation of true stress (σ) as compared to the experimental data from Fig. A1 (up to a maximum engineering strain of $\varepsilon = 2.15$). The various parameters, chosen within the constraints mentioned in the previous paragraph, were: $b = 18$; $N = 30$; $\lambda_s = 1$ at $\varepsilon = 0$ increasing linearly to $\lambda_s = 1.18$ at the end of loading ($\varepsilon = 2.15$); G_0 starting from an original value of $G_{0,\,\text{orig}} = 0.35$ MPa at zero strain (point A: $\varepsilon = 0$) decreasing linearly to 25% of this initial value at the end of loading (point B: $\varepsilon = 2.15$). The gradual decrease in G_0 during the loading corresponds to a 4-fold decrease in the effective cross-link density due to de-tangling of physical entanglements, as discussed in the previous paragraph. The value of υ_{eff}, the effective volume of the hard domain, was treated as an adjustable parameter so that the computed stress $\sigma(\lambda)$ follows the experimental loading curve.

Fig. A4 displays the resulting behavior of υ_{eff} as a function of strain. Although the actual volume fraction of the fillers is only ~ 16% in TR-55, υ_{eff} starts out higher, around 42%. The higher than actual value of υ_{eff} in the beginning of loading can be interpreted as due to an occluded volume of the polymer that effectively behaves like part of the rigid domain. With increasing strain, this occluded volume gets released, thus irreversibly increasing the fraction of the soft domain and correspondingly decreasing the volume fraction of the hard domain. At large strains, one expects the occluded volume to nearly go to zero, in which case υ_{eff} should be around the volume fraction of the fillers originally included in the rubber formulation, consistent with the behavior we see in Fig. A4. Another point of consistency check for this model is to consider the filler-enhancement factor for the mechanical modulus at small strain. By comparing the small-strain-limit of equation (A1) (or (A2)) with that of the strain-amplified materials model (eq. (5)) one obtains the following formula for the enhancement factor (denoted by α):

$$\alpha = (1 - v_{eff})X = (1 - v_{eff})(1 + 3.5v_{eff} + bv_{eff}^2), \qquad \text{(A7)}$$

which, with the choice of b = 18, reduces to the well-known filler-enhancement factor of Guth and Gold. Using the small-strain value $v_{\text{eff}} \sim 0.42$ (see Fig. A4), we obtain $\alpha \sim 3.3$, which is within the range expected from experimental values on a number of filled rubber systems.

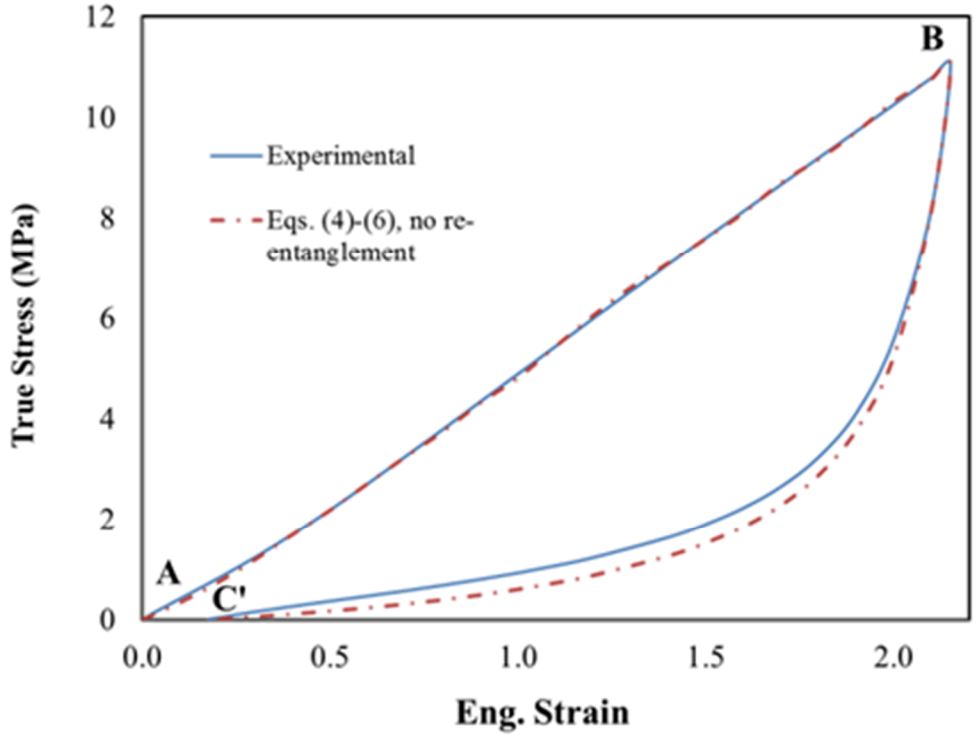

Figure A3. Stress-strain response in TR-55 during the first loading-unloading cycle (maximum engineering strain ε_{max} = 2.15): Experimental vs. Simulated results. The experimental results are from Fig. A1, while the simulated results are obtained using eqs. (A4), (A5), and (A6) (see text) with no re-entanglements allowed during unloading (see Fig. A5). The simulated curve corresponds to fixed parameters b = 18, N = 30; on the loading curve G_0 decreases linearly from 0.35 MPa at point A to 0.09 MPa at point B and then assumed to remain constant during unloading (path BC') and further loading until the previous maximum strain is exceeded.

We note that in Fig. A3 the computed unloading curve consistently falls below the experimental unloading curve. The origin of this could be traced back to the assumption in our model that the initially occluded volume of the soft domain that gets pulled out and the physical entanglements that get detangled during the application of tensile strain are both irreversible, i.e., there is no recovery in either of these quantities during the unloading process. Allowing partial recovery in either or both of these quantities will result in a simulated stress that is much closer to the experimental value. Given that possible retraction of the occluded volume presumably occurs on a much longer timescale than the experimental times, we have considered below the case in which the soft network domain undergoes some physical entanglement during unloading. Fig. A5 displays the behavior of the modulus G_0 (as a fraction of the starting value) during loading and unloading in situations both with and without re-entanglement. The latter case leads to the computed stress-strain curve overlap with the experimental data.

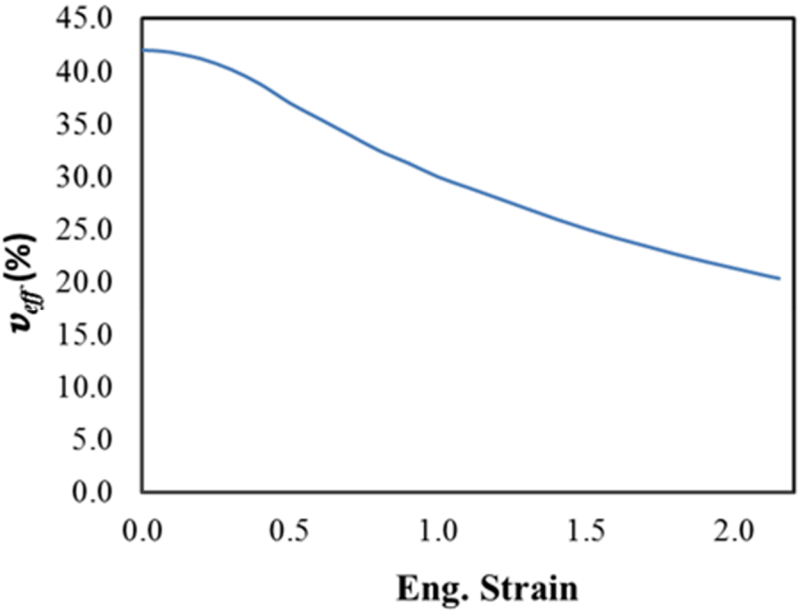

Figure A4. The *effective* volume of the hard domain υ_{eff} as a function of strain during the first loading curve. During subsequent loading and unloading cycles υ_{eff} in this model is assumed to remain at its lowest value (achieved during the previous maximum loading) until the previously attained maximum strain level is exceeded.

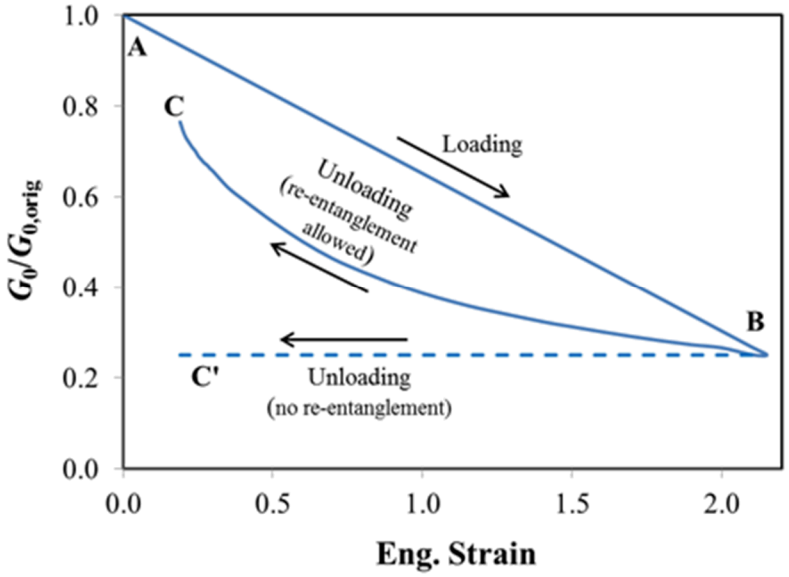

Figure A5. The behavior of modulus G_0 (which can be assumed proportional to the density of cross-links in the soft domain, both physical and chemical) as a function of the applied strain during the first loading and unloading cycle. For unloading two different paths are shown: no re-entanglement allowed (dashed curve BC') that leads to curve BC' in Fig. A3; and re-entanglement allowed (solid curve BC) that leads to a better agreement with experiment. A large fraction of the physical entanglements lost during loading appear to get recovered by the end of unloading.

Summary (Appendix I):

In this Appendix we reported on the development of a phenomenological model that quantitatively reproduces the stress-strain behavior of a specific filled rubber system (TR-55). The model [22] is based on using the Mullins-Tobin concept of amplified strain within the Wang-Guth stress function and incorporates a few additional features that is expected to be generally applicable to most filled rubber systems, including: (1) a permanent set (expressed as recovered length λ_s) that increases linearly as a function of strain (during loading); (2) an effective cross-link density (or modulus G_0) that during loading decreases linearly as a function of strain due to de-tangling of physical entanglements, with partially recovery during unloading; and (3) an effective filler volume that decreases with increasing strain (due to the gradual pulling of the soft polymer domain out of an initial occluded phase) until a saturation value of ~ 16% is reached (corresponding to the filler volume fraction in the TR-55 material). The filler-enhancement factor at small strain is obtained as 3.3, which is within the range of what has been reported in the literature [19] for a number of different filled rubber systems at this filler volume fraction.

APPENDIX II: Parameter values for various models

Constitutive Stress-Strain Model for radiation aging (1D extension with free lateral surfaces)

Notation:

λ = stretch ratio = $1 + \varepsilon$, where ε = engineering strain
$\lambda > 1$ → Tensile strain, $\lambda < 1$ → Compressive strain
$\lambda_1 =$ constant strain at which the material is exposed to radiation
$\sigma(\lambda) =$ True stress [Engineering stress = $\sigma(\lambda)/\lambda$]
$D =$ radiation dosage in Mrad

Without Mullins Effect

Stress-strain relation (up to moderate strain, $\boldsymbol{\varepsilon \sim 50\%}$ or below):

$\sigma(\lambda) = G_0 \frac{(1+C_0 D)}{1+f_D}\left\{\left(\lambda^2 - \frac{1}{\lambda}\right) + f_D\left(\frac{\lambda^2}{\lambda_1^2} - \frac{\lambda_1}{\lambda}\right)\right\}$, where $f_D = e^{\alpha_1 D - \alpha_2 D^2} - 1$;

Recovered Length: $\lambda_s = \left\{\frac{1+f_D\lambda_1}{1+f_D/\lambda_1^2}\right\}^{1/3}$

Permanent Set: $P_s = \frac{\lambda_s - 1}{\lambda_1 - 1}$

Young's modulus: $E = G_0 \frac{(1+C_0 D)}{(1+f_D)}\left[\left(2\lambda_s^2 + \frac{1}{\lambda_s}\right) + f_D\left(2\frac{\lambda_s^2}{\lambda_1^2} + \frac{\lambda_1}{\lambda_s}\right)\right]$

Parameters:

$G_0 =$ 1.5 MPa

$C_0 = 0.054$ Mrad^{-1}

$\alpha_1 = 0.165$ Mrad^{-1}

$\alpha_2 = 0.003$ Mrad^{-2}

Including Mullins Effect

The following model was developed using measurements on SE1700 rubber. We expect this model to be also applicable to TR-55 and other legacy elastomers. As one can see, there are two extra parameters in this model, C_1 and C_2. Below we provide only preliminary estimates of these parameters for TR-55. To obtain more accurate estimates, more elaborate measurements need to be performed (as was done for SE1700).

Stress-strain relation (up to moderate strain, $\varepsilon \sim 50\%$ or below):

$$\sigma = G_0 \frac{(1+C_0 D)}{(1+f_D)} \frac{1}{f_M} \left[\left(\lambda'^2 - \frac{1}{\lambda'} \right) + f_D \left(\lambda''^2 - \frac{1}{\lambda''} \right) \right] ,$$

where $f_D = e^{\alpha_1 D - \alpha_2 D^2} - 1$; $\lambda' = \frac{\lambda}{1+C_1(\lambda_1 - 1)}$; $\lambda'' = \frac{\lambda'}{\lambda_1}$; $f_M = 1 + C_2(\lambda_1 - 1)$

Recovered Length: $\lambda_s = \{1 + C_1(\lambda_1 - 1)\} \left\{ \frac{1+f_D \lambda_1}{1+f_D/\lambda_1^2} \right\}^{1/3}$

Permanent Set: $P_s = \frac{\lambda_s - 1}{\lambda_1 - 1}$

Young's modulus: $E = \lambda_s \frac{\partial \sigma}{\partial \lambda}\Big|_{\lambda = \lambda_s}$

Parameters:

$G_0 =$ 1.5 MPa

$C_0 =$ 0.054 Mrad^{-1}

$\alpha_1 =$ 0.165 Mrad^{-1}

$\alpha_2 =$ 0.003 Mrad^{-2}

$C_1 = 0$ (preliminary)

$C_2 =$ 0.5 (preliminary)

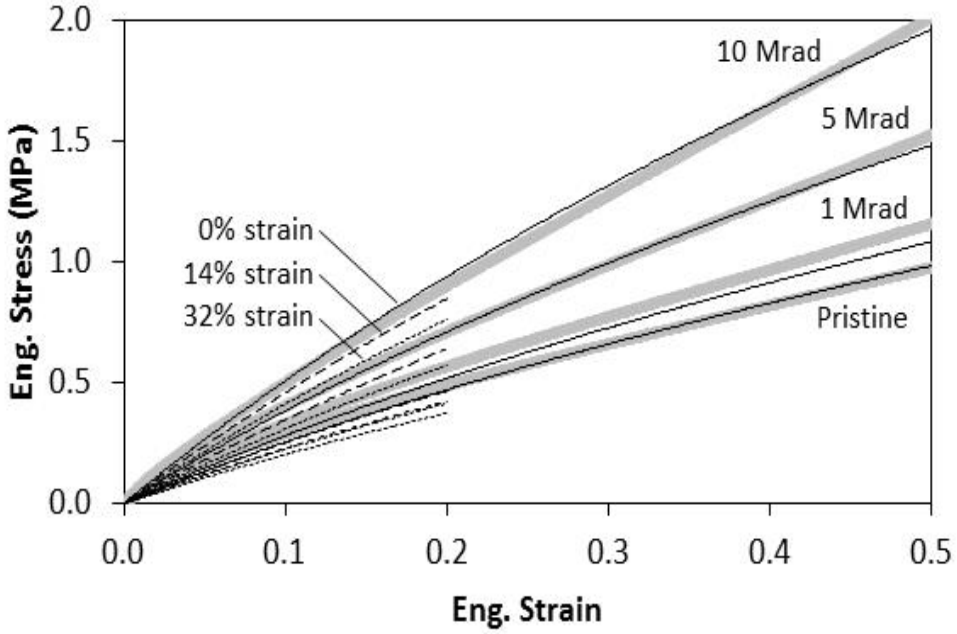

Figure A6. Model prediction for (engineering) stress response for various gamma radiation doses and aging strains (i.e., λ_1) (narrow black lines). Solid line: 0% strain; large dashes: 14% strain; small dashes: 32% strain. The experimental curves at 0% aging strain are shown for comparison (thick gray lines).

Modeling the radiation aging of Molecular Weight Distribution (MWD) between cross-links

(This analysis was performed at $\lambda_1 = 1$)

Notation:

$\nu_0 =$ Volume density of chains between cross-links prior to any radiation dosage

$f_{xl}\nu_0 =$ Density of (new) radiation-induced chains between cross-links

$f_{mod}\nu_0 =$ Density of (old) chains between cross-links that got modified by radiation, either due to new cross-link formation or due to chain scissioning

Then, it can be proven that (for $\lambda_1 = 1$): $f_D = \frac{f_{xl}}{1-f_{mod}}$

Model:

$$f_D = e^{\alpha_1 D - \alpha_2 D^2} - 1 \;\; ; \;\; f_{xl} = \frac{(1+C_0 D) f_D}{1+f_D} \;\; ; \;\; f_{mod} = \frac{f_D - C_0 D}{1+f_D} \;\; ;$$

where $C_0 = 0.054$ Mrad^{-1}, $\alpha_1 = 0.165$ Mrad^{-1}, $\alpha_2 = 0.003$ Mrad^{-2} .

Relationship between f_{mod} and MWD:

Let $n(p,D)$ be the number of chain segment of length p monomers between cross-links when exposed to radiation dosage D. Then, for not-too-large D:

$f_{mod} = \sum_p \{1 - e^{-r_{mod} pD}\} n(p,0) / \sum_p n(p,0)$,

where r_{mod} = rate of modification per monomer per unit radiation dosage.

At $D \ll 1$ we get: $f_{mod} \approx r_{mod} D p_{av}(0)$, where $p_{av}(0) = \sum_p pn(p,0) / \sum_p n(p,0)$, from which we get:

Upon expanding the previous expression of f_{mod} at small D we get: $r_{mod} p_{av}(0) \approx \alpha_1 - 2C_0 = 0.057$ Mrad^{-1}.

The distribution $n(p,D)$ has been obtained from MQ-MMR measurements, as follows.

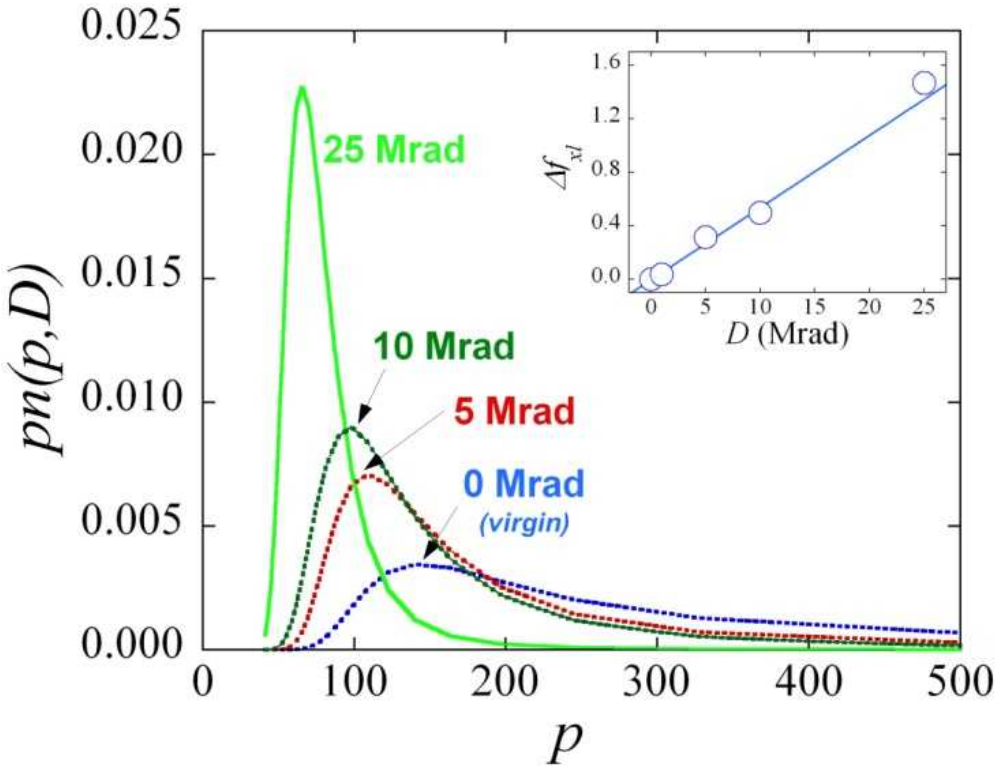

Figure A7. MWD ($pn(p,D)$) from MQ-NMR measurements for various radiation dosages. Inset: Corresponding chain density increment: $\Delta f_{xl} = p_{av}(0)/p_{av}(D) - 1$ as a function of D; solid curve: $y = C_0 D$.

Acknowledgement. We would like to thank Ward Small, Jim Lewicki, Sarah Chinn, Tom Wilson, and Bob Maxwell for their experimental input on which the modeling work was based. This work was performed under the auspices of the US Department of Energy by Lawrence Livermore National Laboratory under Contract DE-AC52-07NA27344.

References:

1. A. V. Tobolsky, I. V. Prettyman, and J. H. Dillon, *J. App. Phys.* 15, 380 (1944); R. D. Andrews, A. V. Tobolsky, and E. E. Hanson, *J. App. Phys.* 17, 352 (1946).
2. D. R. Rottach et al., *Macromolecules* 40, 131 (2007).
3. H. S. Fricker, *Proc. R. Soc. London A* 335, 269 (1973).
4. R. S. Maxwell et al., *Polym. Degrad. Stab.* 94, 456 (2009).
5. K. Saalwächter, *J. Am. Chem. Soc.* 125, 14684 (2003).
6. K. Saalwächter et al., *J. Chem. Phys.* 119, 3468 (2003).
7. J. R. Giuliani, et al., *J. Phys. Chem.* B 111, 12977 (2007).
8. W. Kuhn, F. Grün, *Kolloid-Z.* 101, 248 (1942).
9. A. Maiti, et al., Phys. Rev. E 83, 031802 (2011).
10. T. H. Weisgraber, et al., *Polymer* **50,** 5613 (2009).
11. L. N. Dinh et al*., J. Appl. Phys.* **109**, 094905 (2011).
12. LAMMPS: Large-scale Atomic/Molecular Massively Parallel Simulator, See *http://lammps.sandia.gov*.
13. O. Saito, *J. Phys. Soc. Jpn.* **13**, 198 (1958).
14. A. Maiti et al., *Phys Rev. E.* 83, 062801 (2011).
15. L. Mullins, *Rubber Chem. Technol.* 42, 339 (1969).
16. J. Diani, B. Fayolle, and P. Gilormini, *Eur. Polym. J.* 45, 601 (2009).
17. L. Mullins and N. R. Tobin, J. Appl. Polym. Sci. 9, 2993 (1965).
18. S. Govindjee and J. C. Simo, J. Mech. Phys. Solids 39, 87 (1991).
19. J. S. Bergstrom and M. C. Boyce, Rubber. Chem. Tech. 72, 633 (1999).
20. H. J. Qi and M. C. Boyce, J. Mech. Phys. Solids 52, 2187 (2004).
21. M. C. Wang and E. Guth, J. Chem. Phys. 20, 1144 (1952).
22. A. Maiti et al., *Phys. Rev. E*, 89, 012602 (2014).